THE JOURNAL OF PHYSICAL CHEMISTRY C
A JOURNAL OF THE AMERICAN CHEMICAL SOCIETY

pubs.acs.org/JPCC

Article

Nature of Enhanced Brønsted Acidity Induced by Extraframework Aluminum in an Ultrastabilized Faujasite Zeolite: An *In Situ* NMR Study

Published as part of The Journal of Physical Chemistry virtual special issue "Advanced Characterization by Solid-State NMR and In Situ Technology".

Brahim Mezari, Pieter C. M. M. Magusin, Sami M. T. Almutairi, Evgeny A. Pidko, and Emiel J. M. Hensen*

Cite This: *J. Phys. Chem. C* 2021, 125, 9050–9059

Read Online

ACCESS | Metrics & More | Article Recommendations | Supporting Information

ABSTRACT: The enhancing effect of extraframework Al (EFAl) species on the acidity of bridging hydroxyl groups in a steam-calcined faujasite zeolite (ultrastabilized Y, USY) was investigated by *in situ* monitoring the H/D exchange reaction between benzene and deuterated zeolites by ^{1}H MAS NMR spectroscopy. This exchange reaction involves Brønsted acid sites (BAS) located in sodalite cages and supercages. In a reference faujasite zeolite free from EFAl, both populations of BAS are equally and relatively slowly reactive toward C_6H_6. In USY, in stark contrast, the H/D exchange of sodalite hydroxyl groups is significantly faster than that of hydroxyl groups located in the faujasite supercages, even though benzene has only access to the supercages. This evidences selective enhancement of BAS near Lewis acidic EFAl species, which according to the NMR findings are located in the faujasite sodalite cages.

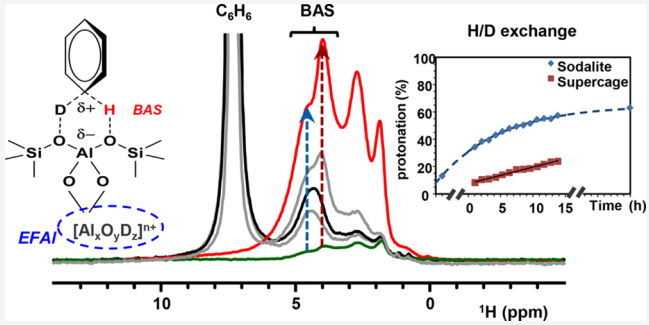

INTRODUCTION

Faujasite zeolite (framework code FAU, zeolite Y, Figure 1) is widely used as an acid catalyst for (hydro)cracking operations in the oil refining industry. In its as-synthesized form, the zeolite has a high density of framework aluminum (FAl) and exhibits only weak intrinsic acidity and limited hydrothermal stability. The Brønsted acidity and stability of such a Y zeolite can be strongly enhanced by removing Al from the framework (dealumination). Dealumination leads to ultrastabilized zeolite Y (USY), which is typically achieved by calcination of as-prepared Y zeolite in the presence of steam at temperatures in the range of 550−800 °C. The higher intrinsic Brønsted acidity of dealuminated zeolite relates to the increased concentration of isolated FAl sites (*i.e.*, no framework Al in the second coordination shell).[1,2] A substantial part of Al atoms extracted from the framework are relocated to positions outside the framework (extraframework Al, EFAl). While typically a part of these EFAl species are removed by further chemical treatment, it is known that residual EFAl species influence the acidity and reactivity of steam-calcined zeolites.[2] This can for instance be

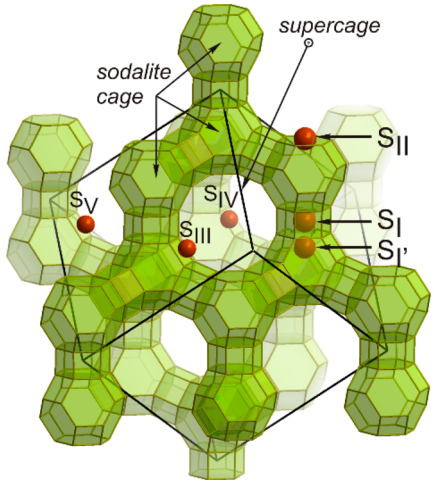

Figure 1. Faujasite unit cell and cation exchange sites. Reproduced with permission from ref 16; copyright 2011 American Chemical Society.

Received: January 14, 2021
Revised: April 7, 2021
Published: April 22, 2021

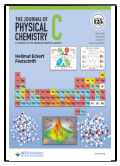

appreciated from the higher intrinsic acidity and acid activity of a USY zeolite in comparison with an EFAl-free zeolite Y reference with a comparable framework Al content, obtained by selective dealumination by ammonium hexafluorosilicate, $(NH_4)_2SiF_6$.[2−7] Although the promoting effect of EFAl species on the acidity of the BAS in USY zeolites has been investigated before,[8−15] important aspects such as the nature of the EFAl species, their location inside the faujasite micropores, and the way they enhance the intrinsic acidity of bridging hydroxyl groups are not understood yet.

Recently, Van Bokhoven et al. demonstrated that EFAl formed during steam calcination of an NH_4Y zeolite predominantly occupies the SI′ sites inside the faujasite sodalite cages (Figure 1a).[17] The structural details of such EFAl species are still unknown. Although most of the previous studies considered cationic mononuclear Al-oxo complexes as EFAl species,[18,19] recent findings indicate that the coordinative unsaturation of such Al centers and the high basicity of the terminal oxygen ligands will cause such complexes to rearrange into multinuclear Al-oxo/hydroxo clusters inside sodalite cages.[20] A recent density functional theory (DFT) study by Liu et al.[21] confirmed that such multinuclear complexes are preferentially located in sodalite cages (Figure S2, Supporting Information). Oxygenated and hydroxylated Al^{3+} cations condense within sodalite cages to form clustered O- and OH-bridged species, bearing a higher formal positive charge compensated through the direct interaction with lattice oxygen anions. In a subsequent work, it was shown that such EFAl species in faujasite strongly affect the acidity of the BAS, leading to a higher activity toward alkane activation.[22]

Solid-state NMR spectroscopy is a powerful technique for studying acid sites in zeolites.[23−25,27] Al NMR spectroscopy can distinguish the different types of Al in zeolites. Recently, White et al. used one- and two-dimensional ^{1}H NMR spectroscopy to directly detect different types of acid sites in HZSM-5 and to reveal direct proton exchange between them.[26] Another possibility lies in the study of probe molecules that interact with the acid sites, *e.g.*, acetone (^{13}C NMR),[27−29] deuterated pyridine (^{1}H NMR),[25] and trimethylphosphine (^{31}P NMR).[30,31] For example, the adsorption of 2-^{13}C-acetone was used as a molecular probe in an NMR study to demonstrate the influence of EFAl on zeolite acidity.[32] In these works, the strong interplay between BAS and EFAl species was emphasized.

Herein, we employ *in situ* NMR spectroscopy to determine the acidity of a Y zeolite by following the H/D exchange of BAS with benzene. The suitability of this method for acidity characterization was first demonstrated by the group of Haw using NMR spectroscopy,[33] while our group later extended this approach using IR spectroscopy.[34] The sensitivity of IR spectroscopy allows quantification of strong BAS in zeolites, clays, and even amorphous silica−aluminas, which contain very few of such acid sites.[35,36] For a range of EFAl-free Y zeolites, Almutairi et al. showed a strong correlation between acidity measured by CO IR spectroscopy and the H/D exchange rate with deuterated benzene as determined by IR spectroscopy.[2] Selective substitution of AlF with Si atoms can be achieved by treating a parent NH_4Y zeolite with ammonium hexafluorosilicate $(NH_4)_2SiF_6$ (AHFS).[1] Thus, the H/D exchange rate can directly indicate the acidity of such an EFAl-free Y zeolite. The much higher H/D exchange rate of Y zeolites promoted by EFAl sites confirmed their enhancing effect on the BAS. Nevertheless, there was no clear correlation between the amount of EFAl sites and the Brønsted acidity. These H/D exchange IR spectroscopy studies showed that protons in sodalite cages exchange at similar rates as those in the more accessible supercages. In the present work, we turn back to ^{1}H NMR spectroscopy to follow the H/D exchange under mild conditions for two Y zeolites, one which was dealuminated by treatment with ammonium hexafluorosilicate such that it is free from EFAl and another one which is a commercial steam-calcined USY zeolite containing EFAl. The nature and location of EFAl species in USY were also investigated by NMR spectroscopy. The peculiar result of our current efforts is that, in the presence of EFAl sites, the sodalite hydroxyl groups exchange substantially faster than the hydroxyl groups located in the faujasite supercages even though benzene has only access to the supercages. The role of EFAl-oxo species stabilized in sodalite cages as acidity-enhancing species will be discussed.

MATERIALS AND METHODS

Sample Preparation. Steam-calcined zeolite USY (Si/Al 4.05) was received from Zeolyst. Dealuminated Y zeolite AHFSY (Si/Al 4.15) was prepared according to a literature procedure involving the isomorphous substitution of Al by Si using ammonium hexafluorosilicate (AHFS).[3]

H/D Exchange. The parent zeolite was dehydrated at 500 °C (heating rate 2 °C/min) for 12 h in a dynamic vacuum ($p < 10^{-5}$ mbar). The dehydrated sample was deuterated by exposure to 10 mbar of D_2O gas at 150 °C for 30 min, followed by evacuation. This procedure was repeated two times. The sample was then evacuated at 450 °C for another 12 h. The two deuterated samples are denoted as D-USY and D-AHFSY. H/D exchange was carried out in a 4 mm zirconium NMR rotor. The dehydrated deuterated zeolite was loaded in the NMR rotor in a glovebox under inert (N_2) atmosphere. The rotor was then placed in a glass tube, connected to a manifold setup, and evacuated for 2 h. Thereafter, the tube containing the sample rotor was cooled to −40 °C, and the sample was brought in contact with a benzene reservoir (partial pressure of 4 mbar) for 1 min. The rotor was then tightly closed with a boron nitride cap and transferred to the NMR probe-head kept at −30 °C.

Solid-State NMR Spectroscopy. NMR measurements were performed on a Bruker DMX500 spectrometer operating at 500, 99, and 132 MHz for ^{1}H, ^{29}Si, and ^{27}Al, respectively. The NMR measurements were carried out using a 4 mm MAS probe-head with a sample rotation rate of 12.5 kHz. ^{1}H NMR spectra were obtained by a Hahn-echo pulse sequence of $p_1-\tau_1-p_2-\tau_1-$aq with a 90° pulse p_1 = 5 μs and a 180° p_2 = 10 μs. The interscan delay was chosen to be 120 s in order to obtain quantitative spectra. The same pulse sequence was used for $T_2(^1H)$ filtered spectra by varying the τ_1 time. $T_{1rho}(^1H)$ filtered spectra were recorded by introducing a lock pulse in the Hahn-echo pulse sequence ($p_1-t_{lock\ pulse}-\tau_1-p_2-\tau_1-$aq) with τ_1 = 2.5 us and a variable $t_{lock\ pulse}$ duration. Two-dimensional ^{1}H MAS NMR exchange experiments were performed using the 90°$-t_1-$90°$-t_{mix}-$90°$-t_2$ pulse sequence with evolution time t_1 and signal detection time t_2. A mixing time t_{mix} of 0.3 and 1 s was used. ^{27}Al NMR spectra were recorded with a single-pulse sequence with a 18° pulse duration of 1 μs and an interscan delay of 1 s. MQMAS spectra were recorded by a three-pulse sequence $p_1-t_1-p_2-\tau-p_3-t_2$ for triple-quantum generation and zero-quantum filtering (strong pulses p_1 = 3.4 μs and p_2 = 1.4 μs at a nutation

https://doi.org/10.1021/acs.jpcc.1c00356
J. Phys. Chem. C 2021, 125, 9050−9059

frequency ν_1 = 100 kHz, a soft pulse p_3 = 11 μs at ν_1 = 8 kHz, a filter time τ = 20 μs, and an interscan delay 0.2 s). ^{27}Al−{^{1}H} TRAnsfer of Population in DOuble Resonance (TRAPDOR)[37] spectra were recorded with the irradiation on and off on the ^{27}Al nuclei of 795 μs, prior to the echo pulse, and an interscan delay of 10 s. Quantitative ^{29}Si NMR spectra were recorded using a high-power proton decoupling direct excitation (DE) pulse sequence with a 90° pulse duration of 3 μs and an interscan delay of 360 s. The ^{1}H and ^{29}Si pulse powers were adjusted to obtain a 90° pulse length equal to 5 μs in tetramethylsilane (TMS). An $Al(NO_3)_3$ solution was used to adjust the ^{27}Al pulse power. The temperature of the sample was controlled by a BVT300 variable temperature control unit and nitrogen gas. For low temperature, the nitrogen gas flow was cooled through a heat exchanger inserted in liquid nitrogen. The appropriate temperature was adjusted by using a heating element in the NMR probe-head. The true temperature inside the probe was calibrated using ethylene glycol and methanol for high and low temperatures, respectively.

X-ray Diffraction (XRD). XRD patterns of zeolites were recorded on a Bruker D4 Endeavor Diffractometer using Cu Kα radiation with a wavelength of 1.54056 Å. 2θ angles from 5 to 60° were measured with a step size of 0.077° and a time per step of 1 s. The catalysts were ground and pressed in sample holders for measurements. Crystallinity of the zeolite samples was calculated from the XRD patterns using the Topas software.

Elemental Analysis. The Al content in zeolite catalysts was determined by elemental analysis, which was carried out by ICP-OES analysis on a Spectro Ciros CCD ICP optical emission spectrometer with axial plasma viewing. For the ICP measurements, the samples were dissolved in a 1.5 mL solution of an $HF/HNO_3/H_2O$ (1:1:1) mixture.

RESULTS

Basic Characterization. The XRD patterns shown in Figure 2a indicate that USY and AHFSY are highly crystalline and exhibit the expected cubic crystal structure with nearly similar lattice constants (Table 1). The correlation between the FAl content in zeolite and the lattice constant can be used to determine the FAl content in zeolite Y.[1,38] Using this method, the FAl contents of the two zeolites were found to be comparable, *i.e.*, 3.0 mmol/g for USY and 3.3 mmol/g for AHFSY.

The ^{27}Al NMR spectrum of the AHFSY zeolite shows one symmetric peak at ∼62 ppm (Figure 3, right top), which can be assigned to FAl. In comparison, the ^{27}Al NMR spectrum of USY contains two additional peaks, *i.e.*, an octahedral Al signal at ∼0 ppm (Figure 3, left top) belonging to EFAl and a broad peak around 40 ppm. The nature of these species was investigated by ^{27}Al MQMAS spectroscopy, which removes the second-order quadrupolar line broadening, thereby enhancing resolution and distinguishing between chemical-shift heterogeneity and quadrupolar broadening. The resulting ^{27}Al MQMAS NMR spectra (Figure 3, left) confirm that USY has both FAl with tetrahedral (T) and octahedral (O) oxygen coordination. The signal at 40 ppm in the 1D spectrum appears as a quadrupolar broadened tetrahedral signal (T′ in Figure 3) in the MQMAS spectrum. This distortion of some tetrahedral FAl is probably caused by the presence of EFAl in USY in the vicinity of FAl as will be confirmed below in ^{1}H 2D correlation NMR experiments.

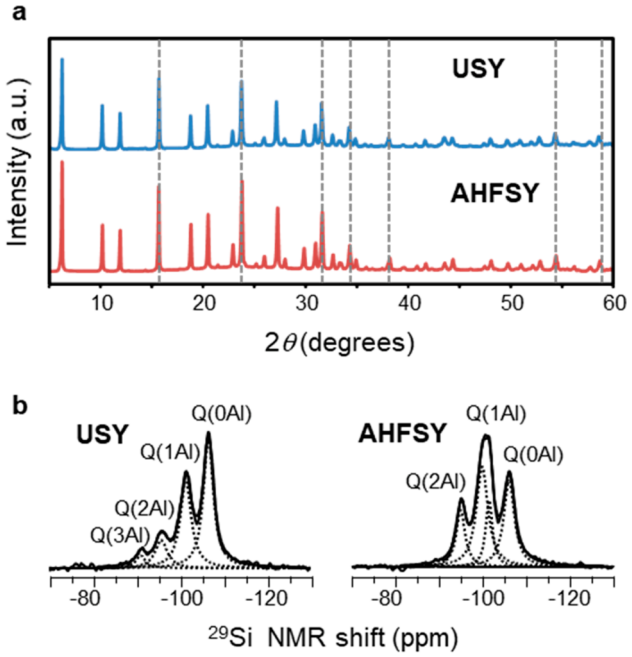

Figure 2. (a) XRD patterns and (b) ^{29}Si MAS NMR spectra of steam-calcined USY and selectively dealuminated AHFSY, respectively. Both XRD and ^{29}Si NMR data are used to determine the framework Al content (Tables 1 and 2).

Table 1. Al Content, c(Al), Derived from ICP, and Framework Al Content, c(FAl), from the XRD Lattice Constant a_0

	c(Al)[a] (mmol/g)	a_0 (Å)	FAl/u.c.[b]	c(FAl)[c] (mmol/g)
USY	4.18	24.477	26	3.0
AHFSY	3.66	24.536	32	3.3

[a]From ICP elemental analysis. [b]Number of FAl atoms per unit cell (u.c.): 107.1(a_0 − 24.238).[1] [c]From FAl/u.c. assuming u.c. composition $Si_{192-n}Al_nO_{384}H_n$.

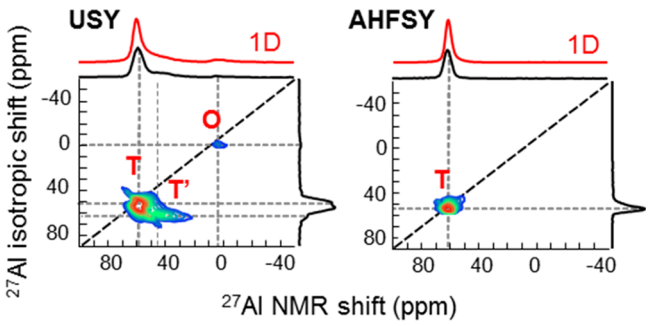

Figure 3. 2D MQMAS ^{27}Al MAS NMR spectra of USY and AHFSY along with projected spectra along the axes. For comparison, quantitative 1D ^{27}Al NMR spectra are plotted at the top (red).

The FAl content can also be estimated from the intensity of the ^{27}Al NMR signal at the tetrahedral position in the 1D spectrum. The calculated FAl content was 1.4 mmol/g for USY and 3.2 mmol/g for AHFSY. However, ^{27}Al NMR spectroscopy is not always accurate in determining the Al population due to the possible NMR invisibility of some Al nuclei, especially in steam-calcined zeolites like USY. To verify these FAl values, we used ^{29}Si MAS NMR spectroscopy as a third method.[39−41] The similar FAl contents of the two zeolite

https://doi.org/10.1021/acs.jpcc.1c00356
J. Phys. Chem. C 2021, 125, 9050−9059

samples are confirmed by the relative occurrences of Si atoms Q^n with different coordinations $Si(OSi)_{4-n}(OAl)_n$ in the zeolite lattice. The respective Si/FAl ratios calculated from the ^{29}Si MAS NMR intensities (Figure 2b) are 5.4 and 4.6, corresponding to 30.1 and 34.1 FAl atoms per unit cell ($T_{192}O_{384}$, T = Si or Al). The framework Al (FAl) contents of USY and AHFSY are thus in the same range (Table 2).

Table 2. ^{29}Si NMR Peak Intensities of Si Atoms with Varying Numbers of Al Neighbors in the Zeolite Lattice and the Framework Al Content, c(FAl), Derived Thereof

	$I^2/I^3/I^4$[a] ^{29}Si NMR	Si/Al[b]	$I^2/I^3/I^4$[c]	c(FAl)[d] (mmol/g)
USY	13/35/47	5.4	16/31/37	2.6
AHFSY	17/53/30	4.6	17/49/24	3.4

[a]Ratio of NMR intensities I^n (%) of Q^n silicon atoms with $Si(OSi)_{4-n}(OAl)_n$ coordination ($I^1 = 100 - I^2 - I^3 - I^4$). [b]Calculated from Si/Al = $\sum I^n / \sum n I^n$.[41] [c]For random Al distribution in lattice without Al−O−Al pairs and Al/Si ratio p: $I^n = 100\binom{4}{n} p^{4-n}(1-p)^n$. [d]From Si/Al, assuming u.c. composition $Si_{192-n}Al_nO_{384}H_n$.

Before studying the H/D exchange between these samples and benzene, we investigate their proton and deuterium forms by ^1H NMR spectroscopy (Figure 4). The resonance at 1.9

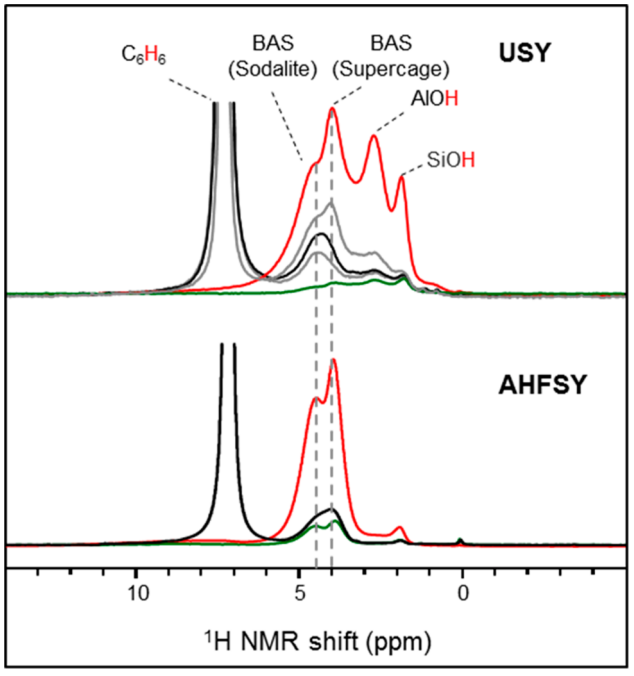

Figure 4. ^1H MAS NMR spectra of dehydrated (top) USY and (bottom) AHFSY in (red) proton and (green) deuterium form as well as (black) loaded with benzene at the start of the H/D exchange at 55 °C. The figure also shows (gray) spectra recorded at 25 and 100 °C.

ppm belongs to silanol moieties, while the signals at 3.9 and 4.6 ppm can be assigned to BAS in the sodalite cages and supercages, respectively. USY shows another signal at 2.8 ppm attributable to EFAl hydroxyl groups. These assignments are supported by the $^1H-^{27}Al$ TRAPDOR effect on the ^1H NMR intensities. TRAPDOR is an NMR technique based on the dipolar coupling between a quadrupolar nucleus, such as ^{27}Al, and a nucleus with spin 1/2 such as ^1H. The technique relies on continuous irradiation of the ^{27}Al spins during a rotor-synchronized spin−echo pulse sequence of the ^1H channel.[37] By comparison of the proton echo intensities in experiments with and without irradiation on ^{27}Al, the extent of the TRAPDOR effect can be monitored. The higher the intensity difference between the two echoes, the greater the dipolar coupling between the two nuclei is, and thus, the closer the two nuclei are. As can be seen in Figure 5, the signals at 2.8

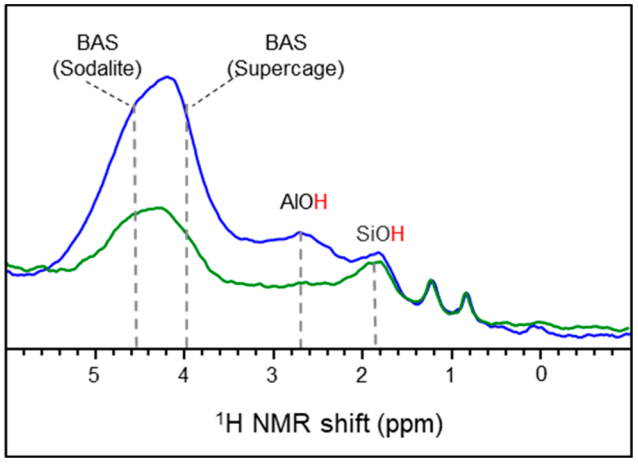

Figure 5. $^1H-\{^{27}Al\}$ TRAPDOR effect in partialy H/D-exchanged USY zeolite. The spectra were recorded at the end of *in situ* H/D exchange at 55 °C (blue and green lines without and with ^{27}Al irradiation, respectively).

and 4.0−4.6 ppm are affected by the irradiation on ^{27}Al and can be assigned to EFAl hydroxyl groups (AlOH species) and BAS groups in supercages and sodalite cages, respectively. The signals at 0.8, 1.3, and 1.9 ppm are respectively attributed to nonacidic silanol groups, arising from framework defects, and to silanol groups.

The ^1H NMR peak intensities for USY and AHFSY (red lines in Figure 4) can be quantitatively interpreted in terms of concentrations (Table 3). As AHFSY contains no EFAl, the

Table 3. Concentration of Proton Species in USY and AHFSY Derived from ^1H NMR Intensities

	δ_H (ppm)	USY mmol/g	AHFSY mmol/g
$BAS_{sodalite}$	4.6	0.57 ± 0.01	1.85 ± 0.01
BAS_{super}	3.9	0.39 ± 0.01	1.40 ± 0.01
Si−OH	1.8	0.13 ± 0.03	0.07 ± 0.01
Al−OH	2.6	0.40 ± 0.01	0.06 ± 0.01

BAS density can be taken equal to the FAl density of 34 $u.c.^{-1}$ as determined by ^{29}Si NMR spectroscopy. The 3.4× lower combined peak area of BAS in USY indicates a BAS density of ~10 $u.c.^{-1}$. The remaining 20 FAl $u.c.^{-1}$ in USY should then be compensated in charge by cationic EFAl species. The overall Al content of USY from ICP equals 48 $u.c.^{-1}$, suggesting that ~18 Al atoms $u.c.^{-1}$ are present as EFAl species. The peak area ratios between the overlapping ^1H NMR signals of the two types of BAS are practically the same for USY and AHSFY within the spectral deconvolution error (Table 3). From the benzene peak area, the total benzene loading before the start of the H/D exchange was 0.31 and 0.50 mmol/g for USY and AHFSY, respectively. This corresponds to, respectively, four and six benzene molecules per unit cell for USY and AHFSY.

https://doi.org/10.1021/acs.jpcc.1c00356
J. Phys. Chem. C 2021, 125, 9050−9059

H/D exchange between the deuterated zeolites and benzene was initially investigated on D-USY at different temperatures. Figure 6 shows a stack plot of the ^{1}H MAS NMR spectra

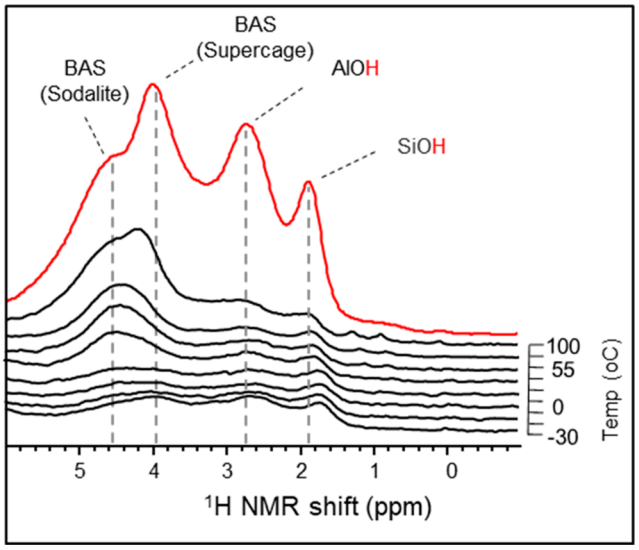

Figure 6. *In situ* ^{1}H NMR of H/D exchange between D-USY and benzene, recorded at different temperatures starting from −30 °C. The spectra were obtained after a specific time at the indicated temperature. Between −30 and 35 °C, the spectra were obtained after 2 h. The 55 °C spectrum was obtained after 14 h of H/D exchange, and the 100 °C spectrum was obtained after 1 h. For comparison, the spectrum of the dehydrated sample is added (red line).

recorded at different temperatures between −30 and 100 °C. The reaction starts at 25 °C with the H/D exchange at the sodalite position followed by H/D exchange of the supercage position. At a temperature of 100 °C, the proton signals of the BAS show an advanced exchange and a peak shape comparable to the fully protonated sample before deuteration and benzene exposure. At this stage, the silanol and EFAl hydroxyl groups are only slightly affected by exposure to benzene, which is expected due to the low acidity of these moieties.[42] The chemical shift of the supercage BAS protons is slightly larger than that of the supercage protons in the zeolites without benzene. In fact, the selective change of this signal confirms its assignment to the supercage BAS protons, because benzene cannot access the sodalite cages and, therefore, mainly interacts with the supercage BAS protons.

The H/D exchange behavior in USY and AHFSY zeolites was then monitored at a constant temperature of 55 °C during 14 h, by recording quantitative ^{1}H NMR spectra each 0.5 h. A series of spectra for USY and AHFSY at different times is given in Figure 7. As can be seen, the total signal intensity of the BAS signal at 4.0 and 4.5 ppm in both zeolites significantly increased during these experiments. A key difference noted is that whereas the sodalite sites in the USY zeolite exchange faster than the supercage sites, these two populations exchange at the same rate in the AHFSY zeolite.

As the sodalite and supercage proton signals overlap, line shape deconvolution was required to obtain quantitative information on the distinct exchange behavior (Figure S3). Deconvolution was done by use of the *dmfit2008* program.[43] A Gaussian line shape was used where the positions and the widths of the sodalite and supercage resonances were kept fixed within the series of spectra. Figure 8 shows the relative

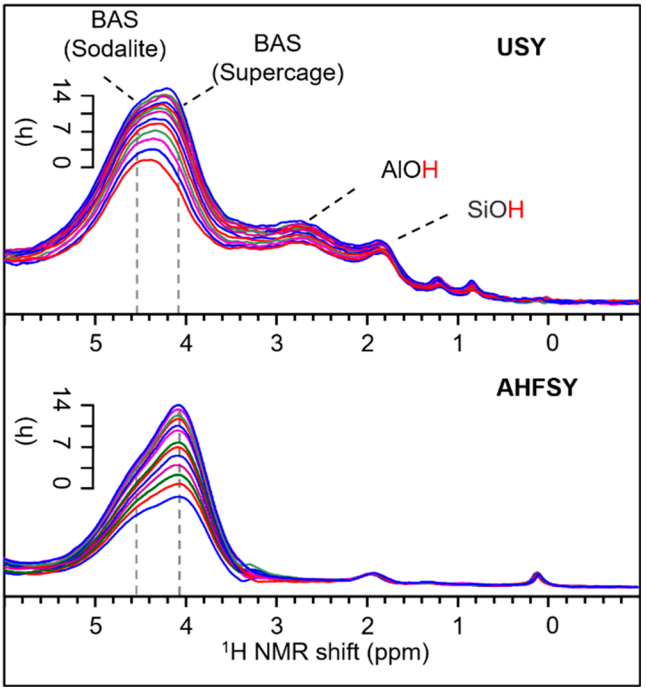

Figure 7. *In situ* ^{1}H NMR of H/D exchange between D-USY and benzene as a function time at 55 °C. Spectra were recorded every 0.5 h up to 14 h in total.

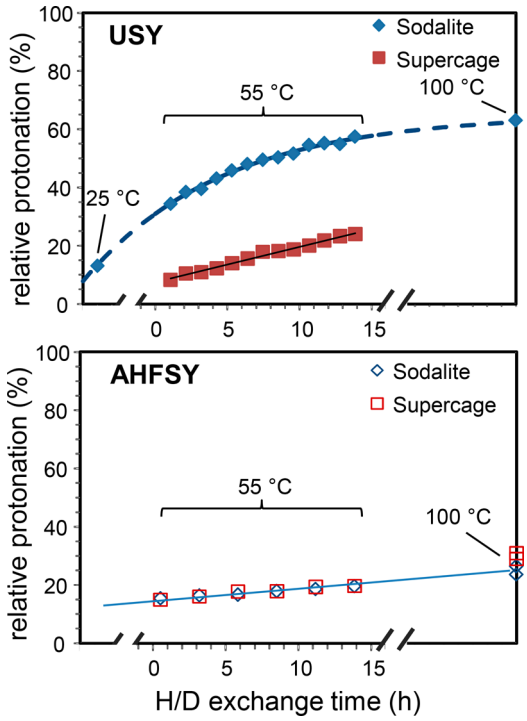

Figure 8. Relative protonation of OD sites in USY and AHFSY based on deconvolution of the *in situ* ^{1}H NMR spectra recorded at 55 °C during H/D exchange of D-USY with C_6H_6 (*cf.*, Figure 7).

increase in the proton signals of BAS of USY and of AHFSY as a function of the exchange time. Confirming the qualitative difference above, the deconvolution confirms that the sodalite and supercage deuteroxyl (OD) sites in AHFSY exchange in the same manner, while for USY, the sodalite OD sites exchange much faster than the supercage OD sites.

https://doi.org/10.1021/acs.jpcc.1c00356
J. Phys. Chem. C 2021, 125, 9050−9059

The faster H/D exchange of sodalite sites is unexpected, because it is well-known that benzene cannot enter the sodalite cages. The exclusive location of benzene in the supercage is confirmed by a selective chemical-shift change of the supercage BAS signal from 3.9 to 4.1 ppm due to benzene, whereas the shift of the sodalite-cage BAS stays unaltered (Figure 9).

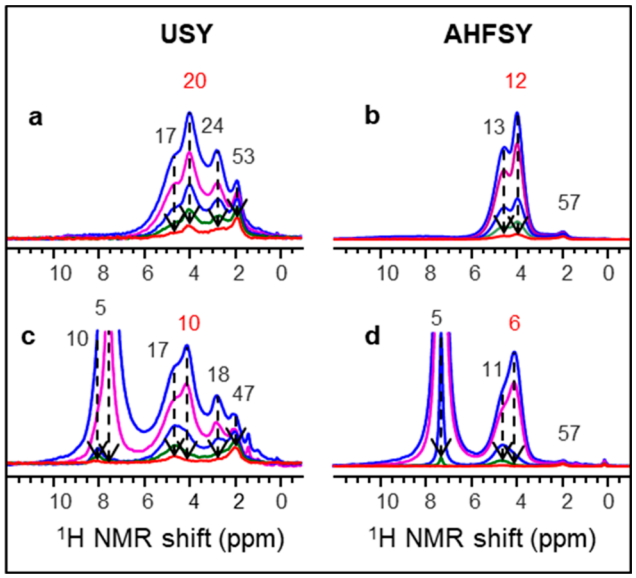

Figure 9. Relative ^{1}H NMR Hahn-echo spectra at varied echo times of fully protonated (a) USY, (b) AHFSY, (c) USY with benzene, and (d) AHFSY with benzene. The used echo times 2τ are 0.005, 2, 20, 40, and 80 ms in the direction of decreasing signal intensity. The numbers above the signals indicate the transversal relaxation time $T_2(^1\mathrm{H})$ determined from the signal decay vs. 2τ.

Furthermore, after benzene absorption, the transversal ^{1}H NMR relaxation is only accelerated for the supercage BAS (Figure 9). The selective relaxation enhancement by a factor of 2 is caused by the dipole interactions between the supercage BAS protons and the relatively high concentration of benzene protons in the supercage. The absence of any benzene-induced relaxation effect on the BAS signal at 4.6 ppm also contradicts any tentative explanation that benzene has accidentally shifted part of the supercage BAS signals underneath the sodalite BAS signal in the ^{1}H NMR spectrum.

2D spin-exchange spectroscopy (2D EXSY) provides information about the proximity of chemically different protons.[26,44] For a sufficiently long mixing time, the protons that are close in space will show cross-peaks in the 2D NMR spectrum. As can be seen in the 2D EXSY spectrum of USY measured at a mixing time of 1 s (Figure 10), the sodalite, supercage, and EF proton spins show such cross-peaks. The relative intensities of these cross-peaks follow the total relative intensities in the sample as can be appreciated from the horizontal section spectra. This means that the proton magnetization at the three sites is mixed within an exchange time of 1 s. USY with adsorbed benzene shows, in addition to the previous exchange picture, cross-peaks with benzene protons. In contrast, the signal due to the silanol does not show cross-peaks with other hydroxyl groups in the zeolite. These findings point to the spatial separation of BAS and EF protons from the silanol groups at the external surface of the zeolite crystallites. Interestingly, in the presence of benzene molecules, the spin-exchange behavior of the EFAl proton

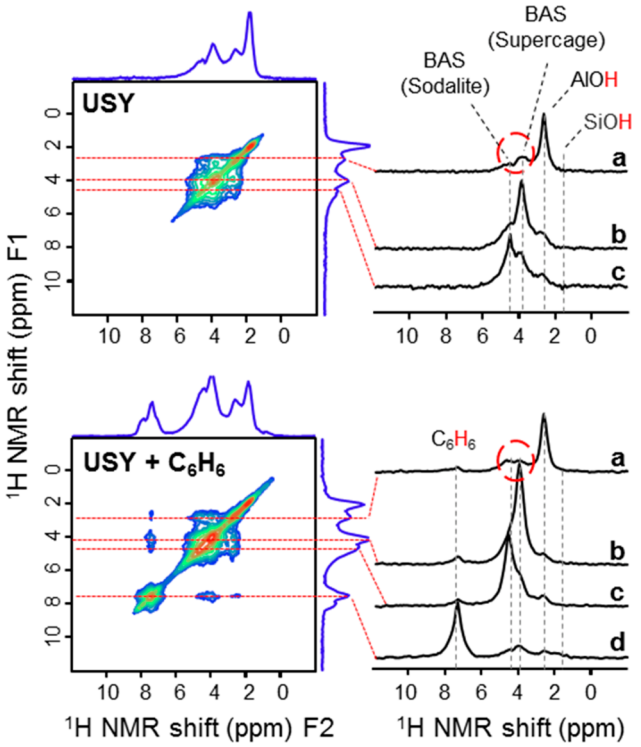

Figure 10. (left) 2D EXSY spectra measured at room temperature for USY with benzene still remaining in the USY sample (bottom) and after the complete removal of benzene (top). The spectra were acquired at a MAS rate of 10 kHz and a mixing time of 1 s. (right) Horizontal sections are shown at F1 ^{1}H NMR shifts corresponding to proton spins of hydroxyl groups associated with (a) EFAl, (b) supercage BAS, (c) sodalite BAS, and (d) C_6H_6.

spins with the supercage spins differs from the exchange without benzene. The amount of the exchanged supercage proton intensity with the EF hydroxyl groups is lower in the presence of benzene, while the intensity of sodalite BAS signal remains the same (*i.e.*, by comparison of the horizontal section in Figure 10). This proves that benzene interacts selectively with BAS in the supercages.

DISCUSSION

For the investigation of the influence of EFAl on the acidity situation in a Y zeolite, an EFAl-containing zeolite USY prepared by steaming was compared to an EFAl-free and chemically dealuminated AHFSY zeolite with comparable Si/FAl ratios. The two samples have similar XRD patterns, reflecting their high crystallinity. The FAl content in AHFSY (Table 1), determined from the XRD lattice constant and ^{27}Al MAS NMR (Table S1) and ^{29}Si MAS NMR (Table 2) spectra are similar and comparable to the total Al content in the sample determined by elemental analysis. This proves that the AHFSY zeolite is free from EFAl. As follows from the ^{27}Al MQMAS NMR spectrum in Figure 3, the steamed USY sample contains octahedrally coordinated EFAl at ~0 ppm, a horizontally broadened peak at ~40 ppm, and a peak at ~56 ppm. The peak at ~40 ppm can be assigned to distorted FAl species.[45] The signal at ~56 ppm lies on the diagonal, which therefore can be attributed to tetrahedrally coordinated FAl^{IV}[45] or FAl species compensated in charge by cationic EFAl instead of protons.[2] The FAl content in USY zeolite determined by ^{27}Al NMR spectra is lower than the value derived from the unit

https://doi.org/10.1021/acs.jpcc.1c00356
J. Phys. Chem. C 2021, 125, 9050−9059

cell volume, which can be attributed to the NMR invisibility of part of Al caused by strong quadrupolar interactions. The number of BAS in USY is 3 times lower than in AHFSY, as can be concluded from a comparison of the peak areas in ^{1}H NMR spectra (Table 3). The distribution of the BAS over the sodalite cages and the supercages is nearly the same in both zeolites. The observed low BAS concentration in USY can be explained by their replacement by cationic EFAl. The high AlOH content as follows from the ^{1}H NMR spectrum of USY is an indication that the cationic EFAl partially appears as $Al(OH)_x^{(3-x)+}$ where x equals 1 or 2. The silanol density in USY is twice that in AHFSY but 3 times lower than the number of AlOH groups. This low silanol density in USY is probably because, parallel to hydrolysis reactions occurring during steaming, a healing reaction between the SiOH groups takes place, leading to siliceous regions.[41] The FAl content in USY and AHFSY, as extracted from XRD lattice constant values, is approximately similar. This forms a good basis for the investigation of the effect of EFAL species on the reactivity of the steamed zeolite. Differences in acidity and reactivity between the two zeolites, which could arise from the effect of framework Si/Al ratio, can therefore be neglected and instead correlated to the effect of EFAl species.

Before discussing the H/D exchange results in detail, some aspects concerning the diffusion and adsorption of benzene molecules in zeolite Y should be clarified. The benzene molecule has a kinetic diameter of ∼6 Å,[46] which is larger than the 6-membered ring (2.3 Å) of the sodalite cages and smaller than the 12-membered ring (7.4 Å) windows of the supercages. Therefore, benzene can freely diffuse in zeolite Y and will exclusively sit in the supercages and the pore windows interconnecting them. This is in line with the observed selective shift change and the decrease in the transversal relaxation $T_2(^1H)$ of the supercage protons due to the presence of benzene. In contrast, the sodalite proton shift and $T_2(^1H)$ relaxation do not change (Figures 6 and 9), implying that benzene cannot enter the sodalite cages. The downfield shift of the supercage signal originates from the effect of the induced magnetic field by the circulating electrons in the benzene aromatic ring.[47] The effective field felt by the supercage protons depends on the orientation of the benzene molecule. When the benzene is facially coordinated to the supercage BAS, the proton will be more shielded, and hence, the peak position will shift upfield. The opposite will happen when the benzene ring and the proton are nearly in the same plane (Figure 11).

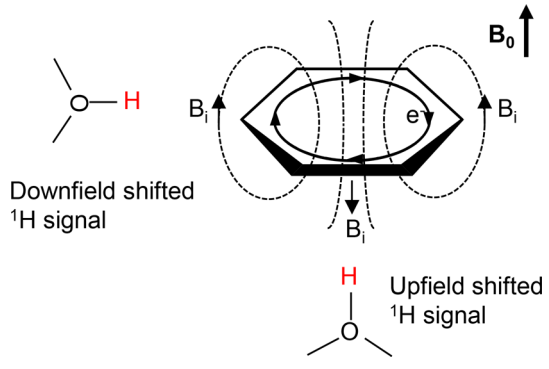

Figure 11. ^{1}H NMR shift dependence on the relative benzene molecule orientation.

This could mean that the peripheral edge of benzene is more oriented in the direction of the supercage BAS such that the protons spend some time in the deshielding region. This configuration could be stabilized by weak or transient complexation of the benzene hydrogen atoms with zeolite oxygen atoms. An alternative explanation could be that the observed small downfield shift is the sum of two effects, namely (i) the upfield shift due to the planar coordination of benzene to the supercage BAS and (ii) a weak hydrogen bond along the molecular C_6 axis.

^{1}H NMR spectroscopy during H/D exchange is a frequently used method to measure the acidity and reactivity of the hydroxyl groups in a faujasite zeolite by monitoring the proton transfer between the BAS and reactants or model molecules, such as benzene.[27,42,48] In all studies we found, however, the researchers focused on the total exchange of the BAS with adsorbed molecules. In the current study, we addressed the site-selective H/D exchange of sodalite and supercage hydroxyl groups. We started from almost completely deuterated zeolites and low benzene loading. Following the H/D exchange at low temperature in this manner provides a good contrast in the H/D exchange reactivity and selectivity of the different hydroxyl sites in the two investigated zeolites.

The USY zeolite showed a higher H/D exchange reactivity with benzene than AHFSY. This behavior agrees with our earlier H/D exchange IR study,[2] which was attributed to the presence of EFAl. Interesting is the exchange of the sodalite BAS with benzene. Although benzene cannot enter the small cages, the sodalite BAS can exchange with molecules that are exclusively sitting in the supercage cavities. This can be explained by perturbation of the local zeolitic structure. These will lead to a flip of the SiO(3)Al and SiO(4)Al bonds in the direction of the supercage, when a guest molecule approaches the inner zeolite wall. The similarity in reactivity between sodalite and supercage BAS in AHFSY (Figure 8 bottom) indicates that all sites possess the same acidity. The faster H/D exchange of the sodalite BAS compared to supercage BAS in USY (Figure 8, top) implies that the reaction of the sodalite BAS is influenced by EFAl species in a different manner than the reaction with the supercage BAS. A possible cause may be the localization of EFAl species in USY zeolite. Van Bokhoven and co-workers[17] showed in their *in situ* XRPD and XAS investigation of the dealumination of NH_4Y by steaming that the formed EFAl species occupy the SI′ site, which is at the external base of the hexagonal prism just inside the sodalite cage. Mota et al.[18,19] mentioned in their work that occupation of the SI′ site in the sodalite cage in the steamed Y zeolite by Al^{3+} close to O(3) oxygen atoms and at the center of the cage (U site) by $Al(OH)_2^+$ leads to an increase in the acid strength of sodalite protons (O(3)H) and a decrease in the supercage (O(1)H) acid strength. They also mentioned that the role of the EFAl is to stabilize the conjugate base, formed upon deprotonation. Florian et al.[16] demonstrated in their work on La in a Y zeolite that La cations are predominantly stabilized within sodalite cages.

To gain more insight in this, more detailed experimental information about the location of EFAl in the zeolite and the interaction between hydroxyl groups and benzene molecules is needed. For this purpose, we applied ^{1}H NMR relaxometry and 2D ^{1}H NMR in this study. Spin−spin or transversal relaxation originates from the dipolar interaction of a spin with local magnetic fields generated by other neighboring ^{1}H spins. This dipolar interaction falls off rapidly as $\sim 1/r^3$ with the

https://doi.org/10.1021/acs.jpcc.1c00356
J. Phys. Chem. C 2021, 125, 9050−9059

distance r between two spins and, hence, is only effective over short distances (<0.5 nm).[49] The similarity in T_2 relaxation behavior between supercage and sodalite-cage protons in AHFSY (Figure 9) indicates that the environments of the protons at the two types of sites are similar. This is in line with the picture outlined above about the similar acidity of the two types of BAS in AHFSY. The high proton density in benzene causes neighboring ^{1}H spins in the supercage to relax faster than without benzene. This reveals valuable information about the relative location of the different hydroxyl groups in the zeolite. With benzene present in the zeolites, the transversal relaxation of the protons in the sodalite cages remains unchanged, whereas the relaxation of the supercage protons becomes roughly twice as fast in both zeolites. This is because benzene can freely pass through the 12-membered ring window, which affects the $T_2(^1H)$ time of the supercage BAS. As a result of the inaccessibility of the sodalite cage for benzene, the $T_2(^1H)$ time of the sodalite BAS remains unaffected. The slight decrease in $T_2(^1H)$ relaxation time of the EFAl OH in USY suggests that the EFAl is positioned further away from the high proton density of benzene in comparison to the supercage BAS. In USY, benzene shows, in addition to the bulk chemical shift around 7.3 ppm, a downfield shift at ~8.0 ppm. An explanation for this shift could be that some of benzene molecules are highly deshielded as result of a stronger H−benzene bond with negative framework oxygen atoms. The appearance of cross-peaks in 2D EXSY ^{1}H NMR spectra between bridged and EFAl hydroxyl groups suggests that the EFAl species are in close proximity to the BAS. The silanol protons show no cross-peaks with the other hydroxyl groups and are therefore exclusively at the external surface of the zeolite crystals. This is in good agreement with the unaltered T_2 of the silanol protons upon benzene adsorption and with the results reported by Mildner and Freude.[42]

In the presence of benzene, the situation outlined above is changed. The cross-peak signal arising from the interaction of the supercage and the EF protons is slightly attenuated (Figure 10). The attenuation of the cross-peak by benzene indicates that a fraction of the EF proton intensity is transferred to benzene. This could be explained by considering EF proton spins exchanging indirectly, via supercage protons, with the benzene. This is again an indication for the selective exchange of benzene with the supercage BAS protons. $T_{1\rho}(^1H)$ relaxometry, which is sensitive to short-range proximity (Figure S1), suggests also that cationic EFAl species are located in close proximity of the sodalite BAS. The H/D exchange behavior between the BAS in USY and benzene as well as the obtained experimental information from $T_2(^1H)$, $T_{1\rho}(^1H)$ relaxometry, and 2D EXSY NMR spectroscopy indicate that the cationic EFAl is located in the sodalite cage.

In Figure 12, the H/D exchange reaction between the BAS and benzene in the presence of EFAl is proposed. Upon deprotonation, the negatively charged zeolite surface is stabilized by a cationic EFAl complex. Consequently, the sodalite BAS reactivity is increased by the presence of EFAL species.

CONCLUSION

We carried out an *in situ* ^{1}H MAS NMR study of the H/D exchange reaction between benzene and BAS in EFAl-free dealuminated AHFSY and steam-calcined USY zeolites with a main focus on unraveling the nature of the promoting effect of

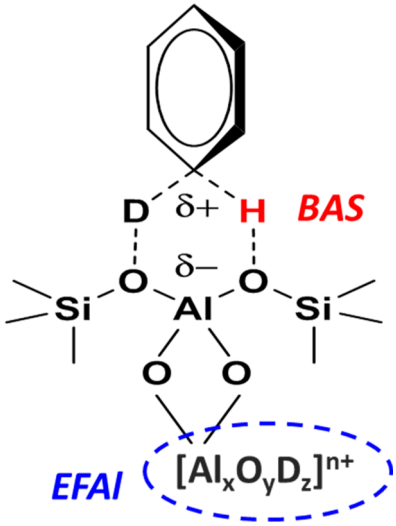

Figure 12. Stabilization of the negatively charged zeolite surface by EFAl cations.

EFAl on zeolitic BAS. The NMR approach here differs from our earlier *in situ* IR spectroscopy approach by starting from the deuterated zeolite instead of the proton form and involving continuous exposure to low benzene concentrations instead of transient pulses at high benzene densities. Benzene selectively changes the ^{1}H NMR chemical shift of the supercage BAS yet does not influence the shift of the sodalite-cage BAS. This is consistent with the accepted picture that C_6H_6 exclusively adsorbs in the supercages, because the sodalite cages are inaccessible for benzene. Nevertheless, in the case of the EFAl-free AHFSY zeolite, our *in situ* NMR study shows that the sodalite and the supercage BAS undergo equally fast H/D exchange. On the contrary, in USY, the H/D exchange of the sodalite-cage BAS is strongly and, more importantly, selectively enhanced compared to that in AHFSY. Already at 25 °C, the sodalite-cage BAS become significantly protonated within a day, and at 55 °C, the H/D exchange under the specific loading conditions (initial $H_{benzene}/D_{BAS}$ ratio ≈ 2) approaches the equilibrium protonation within several hours.

Given the predominant interactions of benzene with the supercage BAS, the most stable supposedly axial binding configuration of C_6H_6 to this BAS type, through weak hydrogen bonding along the benzene C_6 axis, is not of direct importance for the H/D exchange reaction. H/D exchange is most likely controlled by a less stable peripheral binding state with the hydrogen bonding in the benzene plane. In such a configuration, the approachability of sodalite and supercage BAS for benzene located in the supercage may be more comparable. In addition, the local zeolite framework seems sufficiently flexible to allow for temporary flips of the Al−OH−Si bridges, such that the sodalite BAS may transiently point into the supercages. Such lattice flips alone, however, would at most explain roughly equal H/D exchange rates of the two BAS types, as indeed observed for AHFSY. The strong selective enhancement of reactivity of the sodalite-cage BAS in USY thus appears to be caused by the EFAl species in the sodalite cages of this zeolite.

As indicated by the spatial proximity derived from the equal proton spin-diffusion driven $T_{1\rho}(^1H)$ relaxation behavior of protons in the EFAl species and the sodalite-cage BAS, the sodalite-cage BAS closely interacts with the EFAl. This is in

https://doi.org/10.1021/acs.jpcc.1c00356
J. Phys. Chem. C 2021, 125, 9050−9059

line with earlier DFT computations,[21] which showed the preference of EFAl to be stabilized in the faujasite sodalite cages. The promoting role of EFAl cationic species is therefore to stabilize the negative charge on the lattice upon deprotonation of the sodalite BAS. This leads to a strong and selective enhancement of the acidity of the sodalite-cage BAS observed in the *in situ* ^{1}H NMR of H/D exchange in USY.

■ ASSOCIATED CONTENT

Supporting Information

The Supporting Information is available free of charge at https://pubs.acs.org/doi/10.1021/acs.jpcc.1c00356.

Physicochemical properties of materials. Detailed NMR method. Structural models of EFAl in sodalite cages (PDF)

■ AUTHOR INFORMATION

Corresponding Author

Emiel J. M. Hensen − *Laboratory of Inorganic Materials and Catalysis, Department of Chemical Engineering and Chemistry, Eindhoven University of Technology, 5600 MB Eindhoven, The Netherlands;* orcid.org/0000-0002-9754-2417; Email: e.j.m.hensen@tue.nl

Authors

Brahim Mezari − *Laboratory of Inorganic Materials and Catalysis, Department of Chemical Engineering and Chemistry, Eindhoven University of Technology, 5600 MB Eindhoven, The Netherlands*

Pieter C. M. M. Magusin − *Laboratory of Inorganic Materials and Catalysis, Department of Chemical Engineering and Chemistry, Eindhoven University of Technology, 5600 MB Eindhoven, The Netherlands;* orcid.org/0000-0003-1167-3764

Sami M. T. Almutairi − *Laboratory of Inorganic Materials and Catalysis, Department of Chemical Engineering and Chemistry, Eindhoven University of Technology, 5600 MB Eindhoven, The Netherlands*

Evgeny A. Pidko − *Laboratory of Inorganic Materials and Catalysis, Department of Chemical Engineering and Chemistry, Eindhoven University of Technology, 5600 MB Eindhoven, The Netherlands;* orcid.org/0000-0001-9242-9901

Complete contact information is available at: https://pubs.acs.org/10.1021/acs.jpcc.1c00356

Author Contributions

The manuscript was written through contributions of all authors.

Notes

The authors declare no competing financial interest.

■ ACKNOWLEDGMENTS

This research was financially supported by a TOP grant of The Netherlands Organization for Scientific Research (NWO).

■ ABBREVIATIONS

BAS: Brønsted acid site(s); FAl: framework aluminum; EFAl: extraframework aluminum; H/D exchange: hydrogen/deuterium exchange; IR: infrared; ICP-OES: inductively coupled plasma optical emission spectroscopy; NMR: nuclear magnetic resonance (spectroscopy); EXSY: spin-exchange spectroscopy; MAS: magic angle spinning; MQMAS: multiple quantum magic angle spinning; TRAPDOR: TRAnsfer of Population in DOuble Resonance; DFT: density functional theory; XRD: X-ray diffraction; AHFSY: zeolite Y dealuminated by use of amoniumhexafluorosilicate; USY: ultrastabilized zerolite Y; u.c.: unit cell

■ REFERENCES

(1) Sohn, J. R.; DeCanio, S. J.; Fritz, P. O.; Lunsford, J. H. Acid Catalysis by Dealuminated Zeolite Y. 2. The Roles of Aluminum. *J. Phys. Chem.* **1986**, *90* (20), 4847−4851.

(2) Almutairi, S. M. T.; Mezari, B.; Filonenko, G. A.; Magusin, P. C. M. M.; Rigutto, M. S.; Pidko, E. A.; Hensen, E. J. M. Influence of Extraframework Aluminum on the Brønsted Acidity and Catalytic Reactivity of Faujasite Zeolite. *ChemCatChem* **2013**, *5* (2), 452−466.

(3) Holmberg, B. A.; Wang, H.; Yan, Y. High Silica Zeolite Y Nanocrystals by Dealumination and Direct Synthesis. *Microporous Mesoporous Mater.* **2004**, *74* (1−3), 189−198.

(4) Lago, R. M.; Haag, W. O.; Mikovsky, R. J.; Olson, D. H.; Hellring, S. D.; Schmitt, K. D.; Kerr, G. T. The Nature of the Catalytic Sites in HZSM-5 - Activity Enhancement. *Stud. Surf. Sci. Catal.* **1986**, *28* (C), 677−684.

(5) Makarova, M. A.; Bates, S. P.; Dwyer, J. In Situ Modeling of the Enhanced Brønsted Acidity in Zeolites. *J. Am. Chem. Soc.* **1995**, *117* (45), 11309−11313.

(6) Beyerlein, R. A.; McVicker, G. B.; Yacullo, L. N.; Ziemiak, J. J. Influence of Framework and Nonframework Aluminum on the Acidity of High-Silica, Proton-Exchanged Fau-Framework Zeolites. *J. Phys. Chem.* **1988**, *92* (7), 1967−1970.

(7) Carvajal, R.; Chu, P. J.; Lunsford, J. H. The Role of Polyvalent Cations in Developing Strong Acidity: A Study of Lanthanum-Exchanged Zeolites. *J. Catal.* **1990**, *125* (1), 123−131.

(8) Mota, C. J. A.; Martins, R. L.; Nogueira, L.; Kover, W. B. *J. Chem. Soc., Faraday Trans.* **1994**, *90* (15), 2297−2301.

(9) WANG, Q. L.; GIANNETTO, G.; GUISNET, M. Dealumination of Zeolites. *J. Catal.* **1991**, *130*, 471−482.

(10) Mirodatos, C.; Barthomeuf, D. Superacid Sites in Zeolites. *J. Chem. Soc., Chem. Commun.* **1981**, *2*, 39−40.

(11) Fritz, P. O.; Lunsford, J. H. The Effect of Sodium Poisoning on Dealuminated Y-Type Zeolites. *J. Catal.* **1989**, *118* (1), 85−98.

(12) Beran, S. Comparison of Factors Influencing Acidity of Hydroxyl Groups in Zeolites. Quantum Chemical Study. *J. Phys. Chem.* **1990**, *94* (10), 335−337.

(13) Corma, A.; Fornés, V.; Rey, F. Extraction of Extra-Framework Aluminium in Ultrastable Y Zeolites by (NH4)2SiF6treatments. I. Physicochemical Characterization. *Appl. Catal.* **1990**, *59* (1), 267−274.

(14) Lónyi, F.; Lunsford, J. H. The Development of Strong Acidity in Hexafluorosilicate-Modified Y-Type Zeolites. *J. Catal.* **1992**, *136* (2), 566−577.

(15) Li, G.; Pidko, E. A. The Nature and Catalytic Function of Cation Sites in Zeolites: A Computational Perspective. *ChemCatChem* **2019**, *11* (1), 134−156.

(16) Schüßler, F.; Pidko, E. A.; Kolvenbach, R.; Sievers, C.; Hensen, E. J. M.; Van Santen, R. A.; Lercher, J. A. Nature and Location of Cationic Lanthanum Species in High Alumina Containing Faujasite Type Zeolites. *J. Phys. Chem. C* **2011**, *115* (44), 21763−21776.

(17) Agostini, G.; Lamberti, C.; Palin, L.; Milanesio, M.; Danilina, N.; Xu, B.; Janousch, M.; Van Bokhoven, J. A. In Situ XAS and XRPD Parametric Rietveld Refinement to Understand Dealumination of Y Zeolite Catalyst. *J. Am. Chem. Soc.* **2010**, *132* (2), 667−678.

(18) Mota, C. J. A.; Bhering, D. L.; Rosenbach, N. A DFT Study of the Acidity of Ultrastable Y Zeolite: Where Is the Brønsted/Lewis Acid Synergism? *Angew. Chem., Int. Ed.* **2004**, *43* (23), 3050−3053.

(19) Rosenbach, N.; Mota, C. J. A. A DFT-ONIOM Study on the Effect of Extra-Framework Aluminum on USY Zeolite Acidity. *Appl. Catal., A* **2008**, *336* (1−2), 54−60.

(20) Pidko, E. A.; Hensen, E. J. M.; Van Santen, R. A. Self-Organization of Extraframework Cations in Zeolites. *Proc. R. Soc. London, Ser. A* **2012**, *468* (2143), 2070−2086.
(21) Liu, C.; Li, G.; Hensen, E. J. M.; Pidko, E. A. Nature and Catalytic Role of Extraframework Aluminum in Faujasite Zeolite: A Theoretical Perspective. *ACS Catal.* **2015**, *5* (11), 7024−7033.
(22) Liu, C.; Li, G.; Hensen, E. J. M.; Pidko, E. A. Relationship between Acidity and Catalytic Reactivity of Faujasite Zeolite: A Periodic DFT Study. *J. Catal.* **2016**, *344*, 570−577.
(23) Chu, Y.; Xue, N.; Xu, B.; Ding, Q.; Feng, Z.; Zheng, A.; Deng, F. Mechanism of Alkane H/D Exchange over Zeolite H-ZSM-5 at Low Temperature: A Combined Computational and Experimental Study. *Catal. Sci. Technol.* **2016**, *6* (14), 5350−5363.
(24) Pfeifer, H.; Freude, D.; Hunger, M. Nuclear Magnetic Resonance Studies on the Acidity of Zeolites and Related Catalysts. *Zeolites* **1985**, *5* (5), 274−286.
(25) Hunger, M. Multinuclear Solid-State NMR Studies of Acidic and Non-Acidic Hydroxyl Protons in Zeolites. *Solid State Nucl. Magn. Reson.* **1996**, *6* (1), 1−29.
(26) Chen, K.; Abdolrhamani, M.; Sheets, E.; Freeman, J.; Ward, G.; White, J. L. Direct Detection of Multiple Acidic Proton Sites in Zeolite HZSM-5. *J. Am. Chem. Soc.* **2017**, *139*, 18698−18704.
(27) Haw, J. F.; Nicholas, J. B.; Xu, T.; Beck, L. W.; Ferguson, D. B. Physical Organic Chemistry of Solid Acids: Lessons from in Situ NMR and Theoretical Chemistry. *Acc. Chem. Res.* **1996**, *29* (6), 259−267.
(28) Derouane, E. G. Diffusion and Shape-Selective Catalysis in Zeolites. *Intercalation Chemistry* **1982**, 101.
(29) Xu, T.; Haw, J. F.; Munson, E. J. Toward a Systematic Chemistry of Organic Reactions in Zeolites: In Situ NMR Studies of Ketones. *J. Am. Chem. Soc.* **1994**, *116* (5), 1962−1972.
(30) Karra, M. D.; Sutovich, K. J.; Mueller, K. T. NMR Characterization of Bronsted Acid Sites in Faujasitic Zeolites with Use of Perdeuterated Trimethylphosphine Oxide. *J. Am. Chem. Soc.* **2002**, *124* (6), 902−903.
(31) Kao, H.-M.; Liu, H.; Jiang, J.-C.; Lin, S.-H.; Grey, C. P. Determining the Structure of Trimethylphosphine Bound to the Brønsted Acid Site in Zeolite HY: Double-Resonance NMR and Ab Initio Studies. *J. Phys. Chem. B* **2000**, *104* (20), 4923−4933.
(32) Li, S.; Zheng, A.; Su, Y.; Zhang, H.; Chen, L.; Yang, J.; Ye, C.; Deng, F. Brønsted/Lewis Acid Synergy in Dealuminated HY Zeolite: A Combined Solid-State NMR and Theoretical Calculation Study. *J. Am. Chem. Soc.* **2007**, *129* (36), 11161−11171.
(33) Beck, L. W.; Xu, T.; Nicholas, J. B.; Haw, J. F. Kinetic NMR and Density Functional Study of Benzene H/D Exchange in Zeolites, the Most Simple Aromatic Substitution. *J. Am. Chem. Soc.* **1995**, *117*, 11594−11595.
(34) Hensen, E. J. M.; Poduval, D. G.; Ligthart, D. A. J. M.; Van Veen, J. A. R.; Rigutto, M. S. Quantification of Strong Brønsted Acid Sites in Aluminosilicates. *J. Phys. Chem. C* **2010**, *114* (18), 8363−8374.
(35) Poduval, D. G.; Van Veen, J. A. R.; Rigutto, M. S.; Hensen, E. J. M. Brønsted Acid Sites of Zeolitic Strength in Amorphous Silica-Alumina. *Chem. Commun.* **2010**, *46* (20), 3466−3468.
(36) Hensen, E. J. M.; Poduval, D. G.; Degirmenci, V.; Ligthart, D. A. J. M.; Chen, W.; Maugé, F.; Rigutto, M. S.; van Veen, J. A. R. *J. Phys. Chem. C* **2012**, *116*, 21416.
(37) Grey, C. P.; Vega, A. J. Determination of the Quadrupole Coupling Constant of the Invisible Aluminum Spins in Zeolite HY With1H/27A1 TRAPDOR NMR. *J. Am. Chem. Soc.* **1995**, *117* (31), 8232−8242.
(38) Gounder, R.; Jones, A. J.; Carr, R. T.; Iglesia, E. Solvation and Acid Strength Effects on Catalysis by Faujasite Zeolites. *J. Catal.* **2012**, *286*, 214−223.
(39) Fyfe, C. A.; Bretherton, J. L.; Lam, L. Y. Solid-State NMR Detection, Characterization, and Quantification of the Multiple Aluminum Environments in US-Y Catalysts by 27Al MAS and MQMAS Experiments at Very High Field. *J. Am. Chem. Soc.* **2001**, *123* (22), 5285−5291.
(40) Müller, M.; Harvey, G.; Prins, R. Quantitative Multinuclear MAS NMR Studies of Zeolites. *Microporous Mesoporous Mater.* **2000**, *34* (3), 281−290.
(41) Klinowski, J.; Fyfe, C. A.; Gobbi, G. C. High-Resolution Solid-State Nuclear Magnetic Resonance Studies of Dealuminated Zeolite Y. *J. Chem. Soc., Faraday Trans. 1* **1985**, *81* (12), 3003−3019.
(42) Mildner, T.; Freude, D. Proton Transfer between Brønsted Sites and Benzene Molecules in Zeolites H-Y Studied by in Situ MAS NMR. *J. Catal.* **1998**, *178* (1), 309−314.
(43) Massiot, D.; Fayon, F.; Capron, M.; King, I.; Le Calvé, S.; Alonso, B.; Durand, J. O.; Bujoli, B.; Gan, Z.; Hoatson, G. Modelling One- and Two-Dimensional Solid-State NMR Spectra. *Magn. Reson. Chem.* **2002**, *40* (1), 70−76.
(44) Chen, K.; Gumidyala, A.; Abdolrhamani, M.; Villines, C.; Crossley, S.; White, J. L. Trace Water Amounts Can Increase Benzene H/D Exchange Rates in an Acidic Zeolite. *J. Catal.* **2017**, *351*, 130−135.
(45) Li, S.; Zheng, A.; Su, Y.; Fang, H.; Shen, W.; Yu, Z.; Chen, L.; Deng, F. Extra-Framework Aluminium Species in Hydrated Faujasite Zeolite as Investigated by Two-Dimensional Solid-State NMR Spectroscopy and Theoretical Calculations. *Phys. Chem. Chem. Phys.* **2010**, *12* (15), 3895−3903.
(46) Baertsch, C. D.; Funke, H. H.; Falconer, J. L.; Noble, R. D. Permeation of Aromatic Hydrocarbon Vapors through Silicalite-Zeolite Membranes. *J. Phys. Chem.* **1996**, *100* (18), 7676−7679.
(47) Onak, T.; Inman, W.; Rosendo, H.; DiStefano, E. W.; Nurse, J. Aromatic Solvent Induced Nuclear Magnetic Resonance Shift (ASIS) Behavior and Charge Distribution in Cage Boron Compounds. *J. Am. Chem. Soc.* **1977**, *99* (20), 6488−6492.
(48) Huang, J.; Jiang, Y.; Reddy Marthala, V. R.; Wang, W.; Sulikowski, B.; Hunger, M. In Situ1H MAS NMR Investigations of the H/D Exchange of Alkylaromatic Hydrocarbons on Zeolites H-Y, La,Na-Y, and H-ZSM-5. *Microporous Mesoporous Mater.* **2007**, *99* (1−2), 86−90.
(49) Keeler, J. *Understanding NMR Spectroscopy*, 1st ed.; John Wiley & Sons Ltd: Chichester, 2005.

https://doi.org/10.1021/acs.jpcc.1c00356
J. Phys. Chem. C 2021, 125, 9050−9059